Chemical Speciation and Source Attribution of PM_{10} Samples Collected in 2021 at the CDF Monitoring Site

X. Wang[1], J.A. Gillies[1], S. Kohl[1], and G. Nikolich[2]
Division of Atmospheric Sciences, Desert Research Institute, Reno[1] and Las Vegas[2], NV

The attribution of the sources of the particulate matter (≤10 µm aerodynamic diameter, i.e., PM_{10}) measured at the San Luis Obispo County Air Pollution Control District's (SLOCAPCD, hereafter APCD) CDF monitoring site has been the focus of measurement efforts by the APCD and the Scripps Institute of Oceanography, San Diego CA. The results of the analyses by these respective entities show discrepancies, which has made attribution of the PM_{10} to potential sources less certain. To aid in resolving the uncertainty of the source attribution, a PM_{10} measurement campaign was undertaken in 2021. The APCD provided Federal Reference Method (FRM) filter samplers and DRI provided the pre-weighed Teflon-membrane and pre-treated quartz-fiber filters for collecting the samples. DRI subsequently carried out the chemical speciation of the collected filter samples. Using these speciated data, analyses were undertaken to provide Parks an accounting of the source attribution of PM_{10} during this sampling period. Of particular interest are the days that exceeded the State 24-hour mean PM_{10} standard.

Methods

PM_{10} Sampling

24-hour PM_{10} samples were collected every three days at the CDF monitoring site between April and October 2021 (Figure 1). Paired Teflon-membrane and quartz-fiber filters were used to collect the PM_{10} using a Partisol (FRM) sampler. Two Partisol samplers were used in rotation to allow for testing of any sampler-created bias. In addition, filter blank samples were collected on a 1-in-6 day sampling schedule.

Figure 1. The location of the APCD's environmental monitoring stations CDF and Mesa2 with respect to the ODSVRA. The green hashed line demarcates the riding area of the ODSVRA.

Laboratory Chemical Analysis

Detailed laboratory analyses were conducted for each of the PM_{10} filter samples, including mass, elements, ions, carbon fractions, and organic compounds to identify potential source markers and to perform source attribution (Chow and Watson, 2013; Watson et al., 2016).

Teflon-membrane and quartz-fiber filters were shipped to the APCD following preparation at the DRI Environmental Analysis Facility (EAF) (EAF, 2017, 2018, 2020). Filters received from the APCD were equilibrated in a clean room with controlled temperature (21.5 ±1.5 °C) and relative humidity (RH; 35 ±5%) before gravimetric analysis to minimize particle volatilization and aerosol liquid water bias (Watson et al., 2017; EAF, 2021a). Filters were weighed before and after sampling using a XP6 microbalance (Mettler Toledo Inc., Columbus, OH) with a sensitivity of ±1 µg. A radioactive source (500 picocuries of Polonium210) and an electrostatic charge neutralizer were used to eliminate static charge on the filters. A total of 51 elements (from Na to U) were quantified on Teflon-membrane filters using a Panalytical XRF (Model Epsilon 5, Almelo, The Netherlands) (Watson et al., 1999; EAF, 2021b).

Half of each quartz-fiber filter was extracted in distilled deionized water (DDW) and analyzed for eight water-soluble ions, including: chloride (Cl^-), nitrate (NO_3^-), sulfate (SO_4^{2-}), ammonium (NH_4^+), sodium (Na^+), magnesium (Mg^{2+}), potassium (K^+), and calcium (Ca^{2+}) by ion chromatography (Dionex ICS 5000+ IC systems, Thermo Scientific, Sunnyvale, CA) (Chow and Watson, 2017; EAF, 2021c, 2021d). A 0.5 cm^2 punch was taken from the other half of the quartz-fiber filter to quantify organic carbon (OC), elemental carbon (EC), and eight thermal fractions (OC1-OC4, pyrolyzed carbon [OP], EC1-EC3) following the IMPROVE_A thermal/optical protocol using the DRI Model 2015 Multiwavelength Carbon Analyzer (Magee Scientific, Berkeley, CA) (Chen et al., 2015; Chow et al., 2007; EAF, 2021e). Methyl methanesulfonate ($CH_3SO_3^-$), a marker species for oceanic biogenic materials, was measured using ion chromatography (EAF, 2021c, 2021d).

Standard Operating Procedure documents for the analysis methods (i.e., EAF, 2017, 2018, 2020, 2021a, 2021b, 2021c, 2021d, 2021e) are available upon request. Filter-based PM_{10} samples were collected in accordance with the requirements of US EPA Designation RFPS-1298-127 for PM_{10} sample collection (US EPA, 2022), and following the instrument manual and the California Air Resources Board's Standard Operating Procedure, AQSB SOP 404 (CARB 2020).

Results

A total of 52, 24-hour samples were taken between April and October 2021 at the CDF monitoring site (Figure 2) of which 47 were considered valid. Of these, eight equaled or exceeded the State 24-hour mean PM_{10} mass concentration standard (50 µg m^{-3}) based on the gravimetric measurement of mass and flow volume of the sampler.

Fresh and Aged Sea Salt

Inorganic ions in this costal environment without major local aerosol sources likely come from sea salt, mineral dust, and regional/urban background. Figure 3 shows that measured cations are highly correlated with anions (R^2 = 1.00) with a regression slope of 1.03, indicating that most ions are measured with high precision and particles are nearly neutral. The slightly higher than unity slope (1.03) is dominated by a few data points with high ion concentrations, which is probably caused by carbonate (CO_3^{2-}) that is common in mineral dust but not analyzed for in this study.

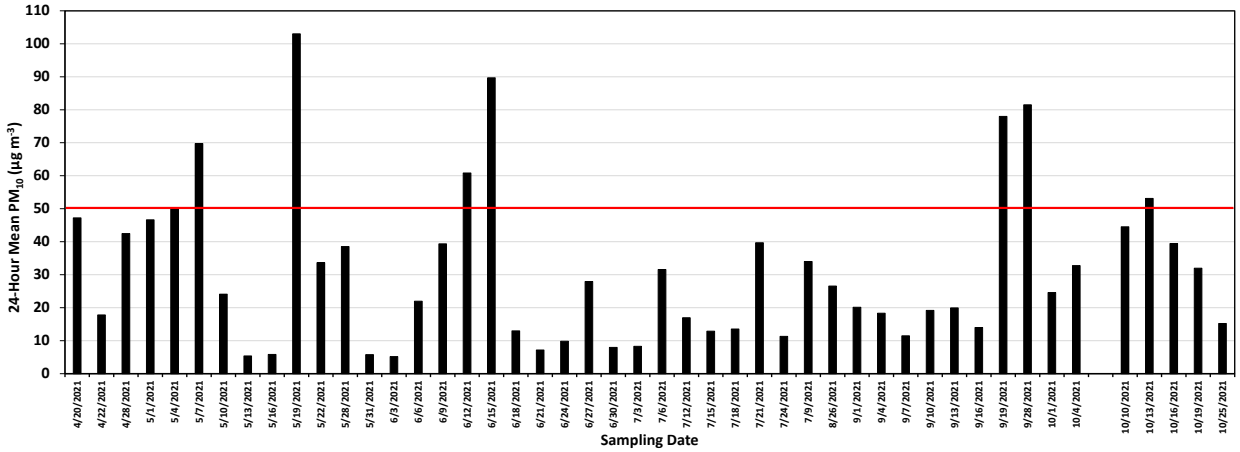

Figure 2. The mean 24-hour PM_{10} (µg m^{-3}) concentration for the days sampled between April and October 2021. Concentration of PM_{10} was determined from gravimetric analysis of the Teflon-membrane filter. The red line represents the State mean 24-hour PM_{10} standard of 50 µg m^{-3}.

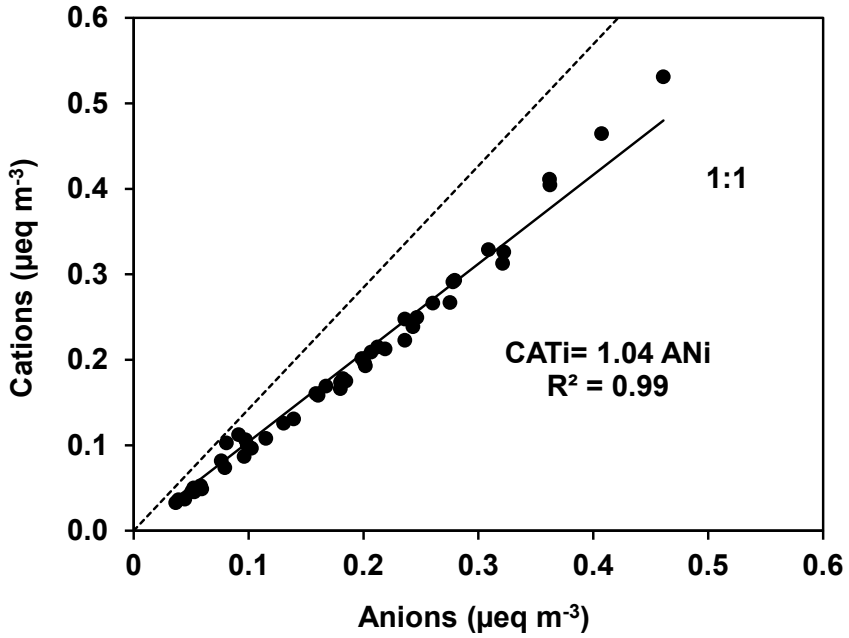

Figure 3. Correlation between cations and anions.

Figure 4 shows that both Mg^{2+} and K^{+} are highly correlated (R^2>0.98) with Na^{+}, and the regression slopes are very close to the expected mass concentration ratios in sea water (Seinfeld and Pandis, 2012). Therefore, Na^{+}, Mg^{2+}, and K^{+} mainly originate from fresh sea salt (Bardouki et al., 2003). By contrast, Figure 5 shows that Ca^{2+} and SO_4^{2-} exceed the fresh seawater ratios for most samples and their correlations with Na^{+} are lower than those in Figure 4. The excess Ca^{2+} and SO_4^{2-} indicate additional sources, likely mineral dust for Ca^{2+} and regional/urban background for SO_4^{2-}. Water soluble Ca^{2+} and

SO_4^{2-} can also form from heterogeneous reactions between sulfuric acid (H_2SO_4) or sulfur dioxide (O_2) and mineral dust (Pakkanen, 1996; Usher et al., 2003; Zhuang et al., 1999).

Chloride depletion from sea salt particles is often observed in coastal regions, where the particulate chloride is displaced as hydrogen chloride (HCl) to the gas phase in atmospheric reactions with nitric and sulfuric acids (McInnes et al., 1994):

$$HNO_3\,(g) + NaCl\,(p) \rightarrow NaNO_3\,(p) + HCl\,(g) \quad (1)$$

$$H_2SO_4\,(g) + 2NaCl\,(p) \rightarrow Na_2SO_4\,(p) + 2HCl\,(g) \quad (2)$$

Assuming sea salt is the only source of Na^+ and Cl^- at the monitoring site, typical fresh sea salt particles have a Cl^-/Na^+ mass ratio of 1.8 (Seinfeld and Pandis, 2012). Figure 6a shows that at the CDF site, the average Cl^-/Na^+ ratio is 1.51, lower than 1.8 for all samples. Therefore, approximately 16% Cl^- has been displaced by stronger acids (e.g., nitric and/or sulfuric acids).

As Na^+ is conservative during sea salt aging, we separate the sea salt Na^+ ($ssNa^+$) as fresh sea salt Na^+ ($fsNa^+$) and aged sea salt Na^+ ($asNa^+$). The fresh sea salt (FS) is calculated as the sum of measured Cl^- that has not been displaced, the corresponding $fsNa^+$ with the same Na^+/Cl^- ratio in seawater, and sea salt (ss) contributions of Mg^{2+}, K^+, Ca^{2+}, and SO_4^{2-}. As $ssMg^{2+}$, ssK^+, $ssCa^{2+}$, and $ssSO_4^{2-}$ do not change with aging, these ions are estimated using their ratios with total measured $ssNa^+$ in typical fresh seawater (Cheung et al., 2011; Lowenthal and Kumar, 2006; Seinfeld and Pandis, 2012). The equation for estimating FS is:

$$FS = fsNa^+ + Cl^- + ssMg^{2+} + ssK^+ + ssCa^{2+} + ssSO_4^{2-} \quad (3)$$

where $fsNa^+$ is estimated as $0.56\times Cl^-$, $ssMg^{2+}$ as $0.12\times ssNa^+$, ssK^+ as $0.036\times ssNa^+$, $ssCa^{2+}$ as $0.038\times ssNa^+$, and $ssSO_4^{2-}$ as $0.252\times ssNa^+$.

The aged sea salt (AS) is estimated by balancing the excess Na^+ with NO_3^- and then with SO_4^{2-} (Zhuang et al., 1999). The excess Na^+ is calculated as the molar equivalent difference between Na^+ and Cl^- (Bardouki et al., 2003). Figure 6b shows that most data points are below the 1:1 line, indicating that both NO_3^- and SO_4^{2-} are involved in Cl^- displacement for most samples. The equation for estimating AS is:

$$AS = asNa^+ + asNO_3^- + asSO_4^{2-} \quad (4)$$

where $asNa^+ = ssNa^+ - fsNa^+$, and $asNO_3^-$ and $asSO_4^{2-}$ are calculated by balancing $asNa^+$.

Figure 7 shows that the AS/FS ratio decreases with PM_{10} concentration when the PM_{10} concentrations are lower than approximately 40 $\mu g\ m^{-3}$, and the ratio remains $\lessapprox 0.2$ at higher PM_{10} concentrations, indicating that FS dominates SS during high PM_{10} concentration events.

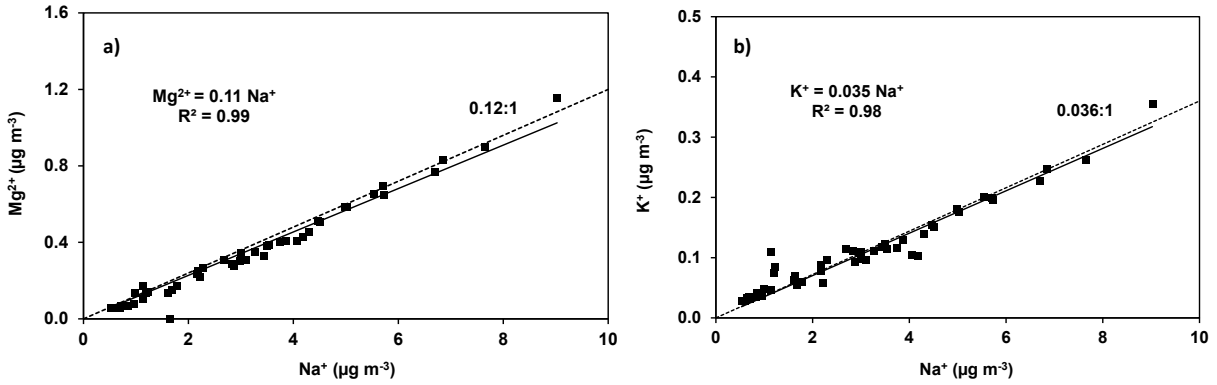

Figure 4. Correlations between: (a) Mg^{2+} and Na^{+} and (b) K^{+} and Na^{+}. The dashed lines indicate ion ratios in fresh seawater.

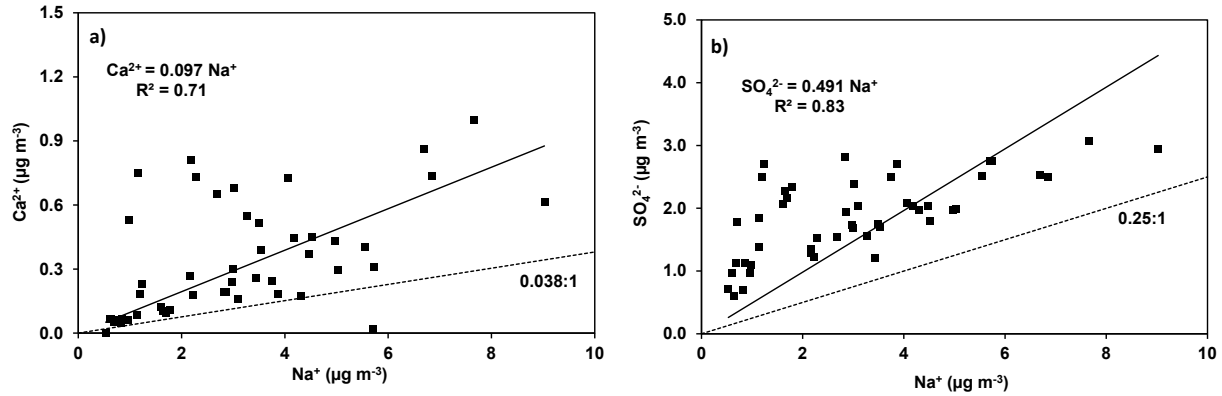

Figure 5. Correlations between: (a) Ca^{2+} and Na^{+} and (b) SO_4^{2-} and Na^{+}. The dashed lines indicate ion ratios in fresh seawater.

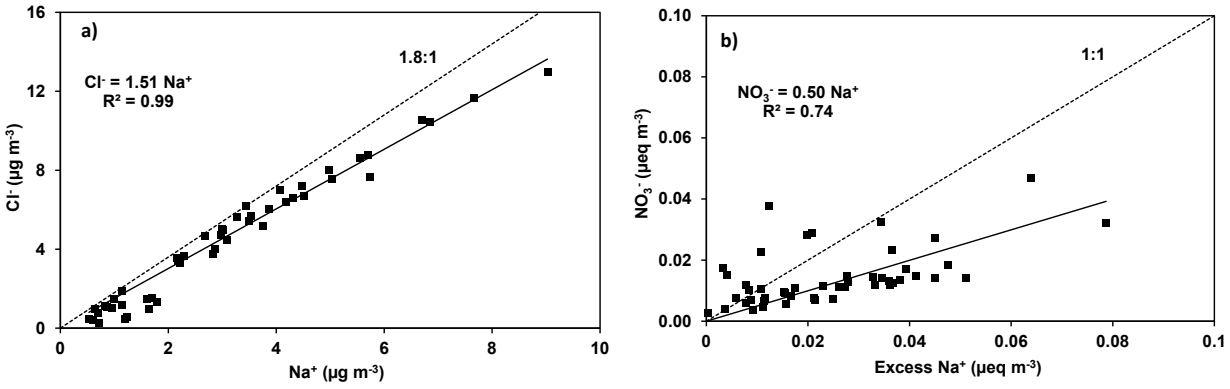

Figure 6. Correlations between: (a) Cl^{-} and Na^{+} and (b) NO_3^{-} and excess Na^{+}.

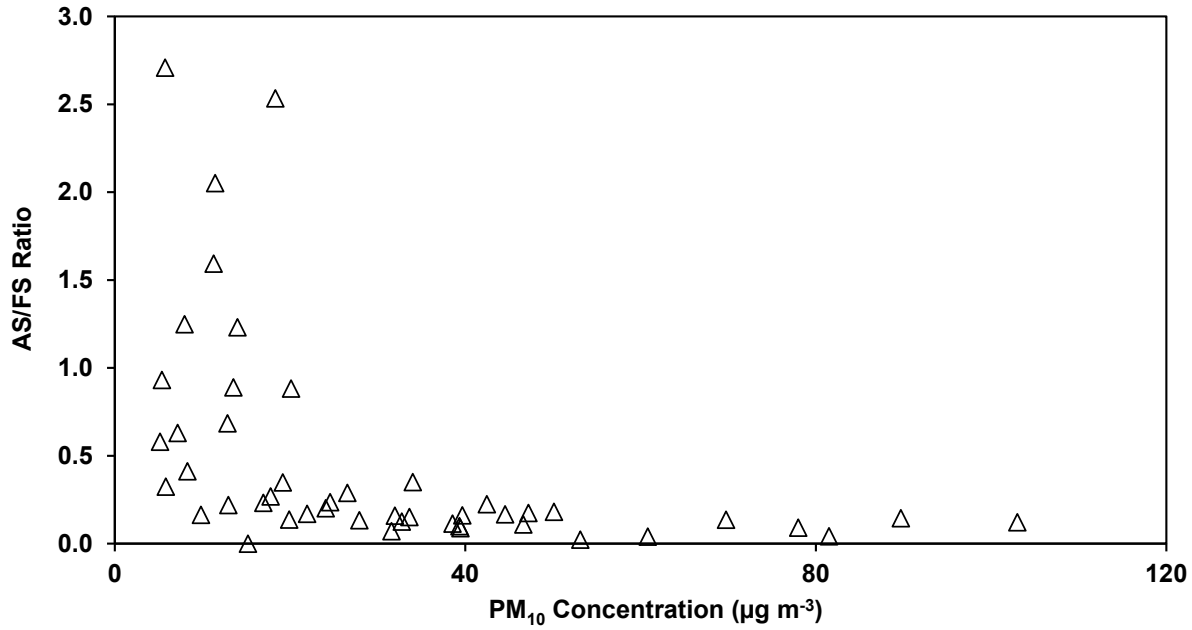

Figure 7. Ratio of aged over fresh sea salt (AS/FS) as a function of PM_{10} concentration.

Filter Blank Speciation

To quantify the potential influence of particles present before sampling and due to particles collecting on the Teflon-membrane and quartz-fiber filters during transport to and from the field site. Filter blanks (filters transported to and from but not used) were analyzed using the same procedures as used for the sample day filters. Five filter blank samples were collected over the course of the May to October 2021 sampling period.

Mean concentrations of the elemental, ionic, and carbonaceous species for the five filter blanks were compared with concentrations of the same species for the days with the lowest 24-hour mean PM10 concentration (6/3/2021, 5 µg m^{-3} ±0.3 µg m^{-3}), highest PM_{10} exceedance day (5/19/2021, 103 µg m^{-3} ±2.1 µg m^{-3}), and the lowest PM_{10} exceedance day (5/4/2021, 50 µg m^{-3} ±1.0 µg m^{-3}). For each of these cases the mean concentrations of the elemental, ionic, and carbonaceous species on a filter blank is much less than the mean concentration on these three sample days. Comparison of the mean blank concentration with the measured sample day concentrations for these three days are shown in Fig. 8. These results provide confidence that the sample day PM10 speciation, as a function of the measured constituents, is not influenced by contamination on the filters during transport.

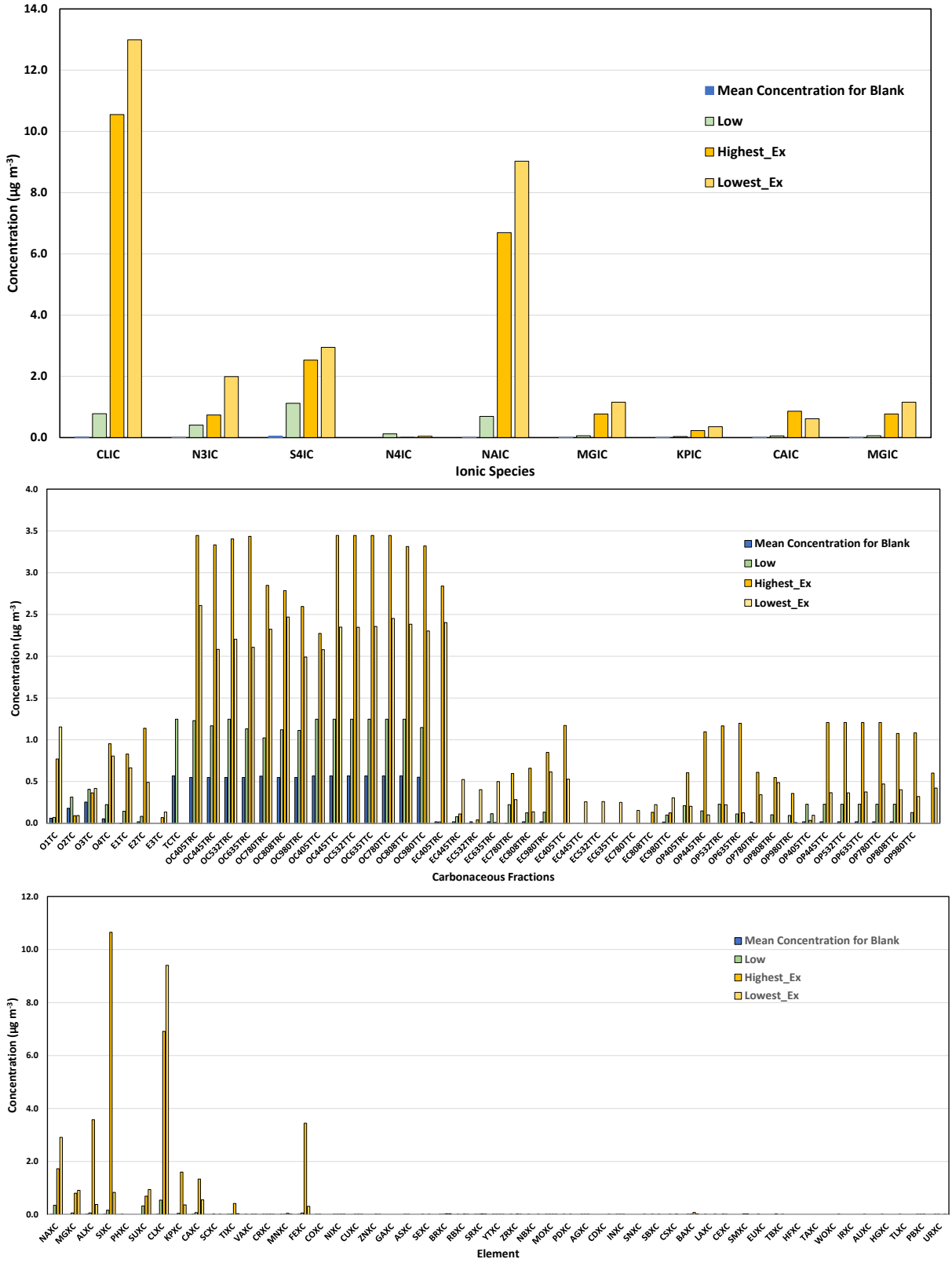

Figure 8. Comparison of the mean blank concentrations with three sample day concentrations: lowest mean 24-hour PM_{10}, highest exceedance day, and lowest exceedance day.

PM_{10} Major Chemical Composition and Mass Reconstruction

Measured PM_{10} species were grouped into seven major compositions, including fresh sea salt (FS), aged sea salt (AS), non-sea salt sulfate ($nssSO_4^{2-}$) that is estimated as the total SO_4^{2-} minus the sea salt SO_4^{2-} ($ssSO_4^{2-}$), mineral dust (MD), elemental carbon (EC), organic matter (OM = OC × multiplier), and other measured species. The sum of these seven composition groups is defined as the reconstructed mass, and the difference between the gravimetric and reconstructed mass is reported as the "unidentified" mass (Chow et al., 2015).

FS and AS are estimated using Eqs. 3 and 4, respectively. The MD is estimated as:

$$MD = 3.48\times Si + 1.63\times nssCa + 2.42\times Fe + 1.94\times Ti \quad (5)$$

following the modified IMPROVE formula, where non-sea salt Ca (nssCa) is the total Ca minus the sea salt Ca^{2+} ($ssCa^{2+}$) in Eq. 3 (Chow et al., 2015; Simon et al., 2011).

A multiplier of 1.8 is used to convert OC to OM for non-urban aerosols (Hand et al., 2011; Simon et al., 2011). The "other" category is the sum of other measured ions (e.g., NH_4^+) and elements (e.g., Br and Ba) without double counting. The reconstructed mass (RM) is calculated as:

$$RM = OM + EC + nss\ SO_4^{2-} + FS + AS + MD + Others \quad (6)$$

The relation between the mass determined by gravimetric analysis and the reconstructed mass (Figure 9) shows a strong correlation ($R^2 = 0.99$) indicating that the gravimetric and chemical measurements are of a high quality. We note that the reconstructed mass data for 10/7/2021 (shown as the open red triangle), an identified exceedance day, is quite different from the other days. Upon inspection we could not identify any anomalous features of the filters nor any issues with the analytical procedures that would suggest why this day is an outlier in terms of chemical speciation and hence much lower reconstructed mass. This datum is treated as an outlier and not included in the linear regression. Since the slope (0.84) of the best-fit linear regression line is less than unity, it indicates that there are constituents of the PM_{10} that are not accounted for by those measured in the laboratory analysis or in the mass reconstruction (Eq. 7). The unidentified mass is also shown as the difference between the gravimetric mass (represented by *) and the reconstructed mass (represented by the stacked bar height) in Figure 9. The attribution of the unidentified PM_{10} mass to a source is described later in this report.

Figure 10 shows that mineral dust and sea salt have high concentrations during the high PM_{10} days at the CDF monitoring station, representing major influences from the ocean and saltation driven dust emissions, while OM is a minor contributor. Additionally, the concentrations of tracers for on-road traffic emissions (represented by EC) and regional pollution (represented by $nssSO_4^{2-}$, $nssNO_3^-$ and NH_4^+ (included in Others category)) are low. The concentration of methyl methanesulfonate ($CH_3SO_3^-$) was <1.2 μg m^{-3} for all sampling days. The PM_{10} mass percentages of chemical constituents in Figure 11 show that while sea salt and mineral dust are the dominant PM_{10} constituents during high PM_{10} concentration days, organics and $nssSO_4^{2-}$ contributions are higher during lower PM_{10} concentration days.

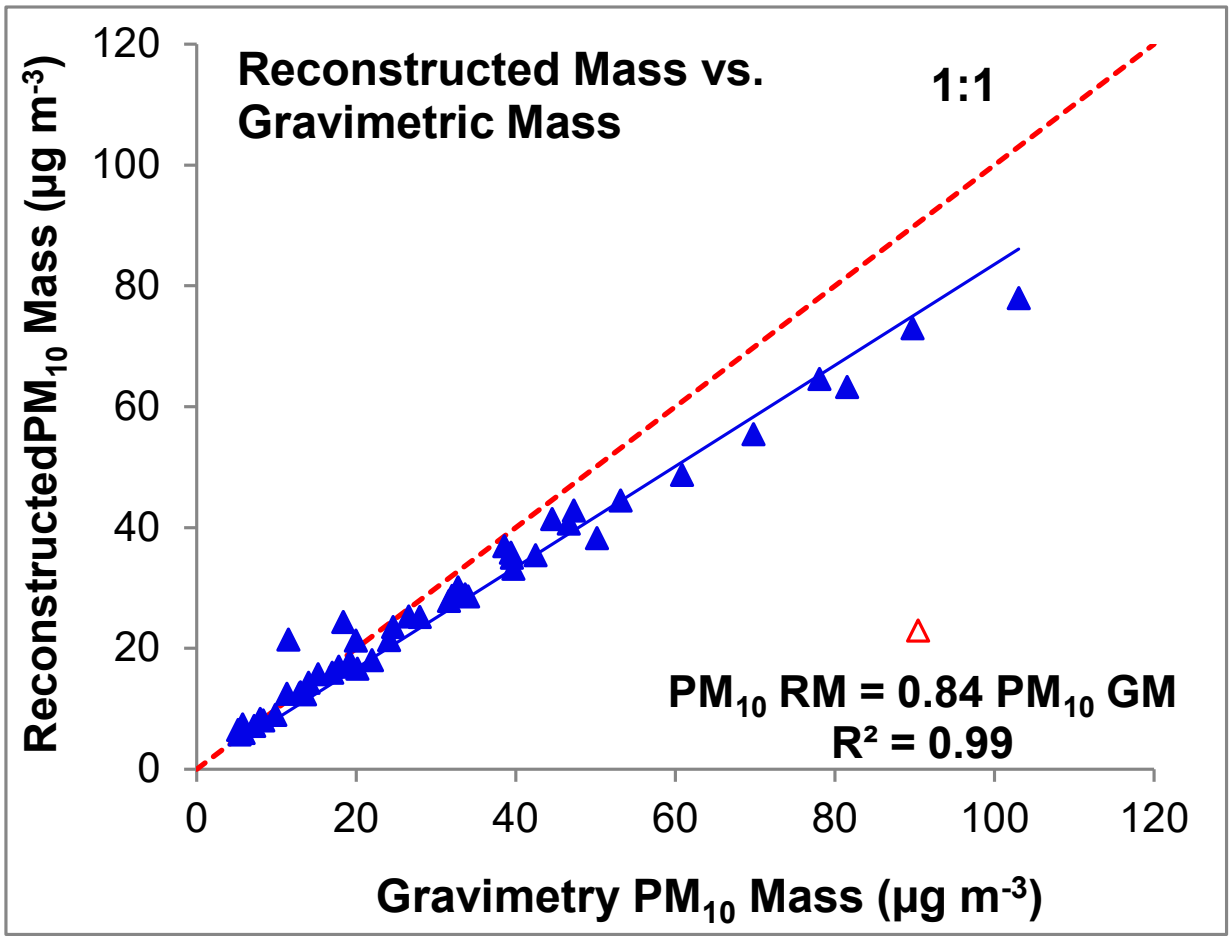

Figure 9. Correlation between reconstructed and gravimetric PM_{10} mass concentrations. The open red triangle in the relation shown in the top panel (sampling day 10/7/2021) is deemed as an outlier and not included in the linear regression.

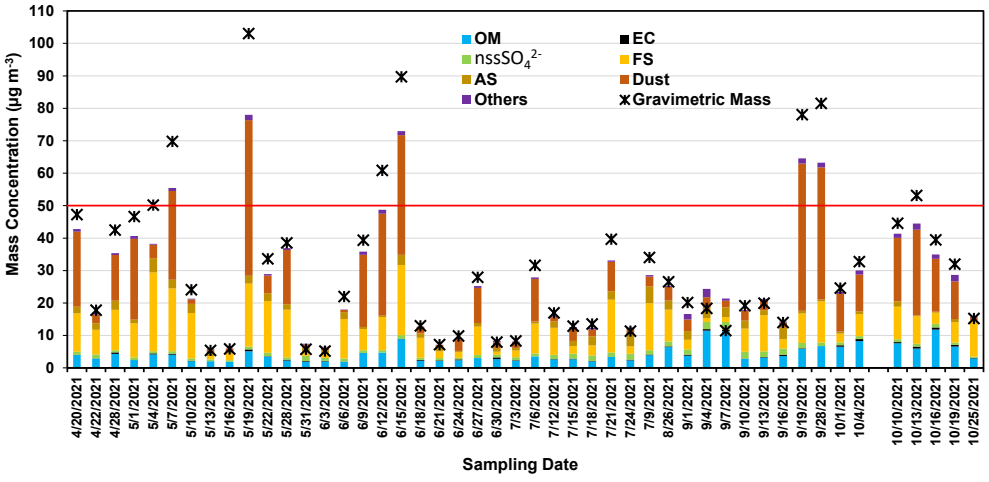

Figure 10. Concentration of PM_{10} chemical constituents (stacked bars) and gravimetric mass (*) for the days sampled between April and October 2021. The red line represents the State mean 24-hour PM_{10} standard of 50 µg m^{-3}.

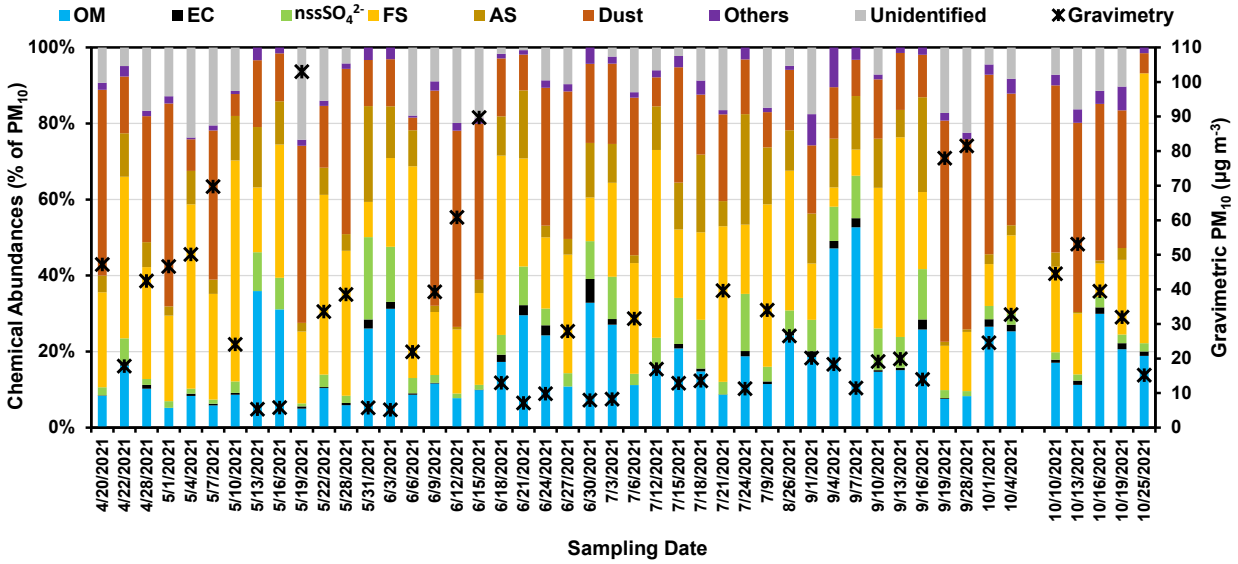

Figure 11. PM_{10} mass percentage of chemical constituents (stacked bars) and gravimetric mass (*) for the days sampled between April and October 2021.

Source Attribution of PM_{10} at CDF

Of critical interest for understanding the potential contributions to PM_{10} originating from the direction of the ODSVRA that is measured at CDF is the identification of days that exceed the State mean 24-hour PM_{10} standard. During the monitoring period eight exceedance days were identified (Figure 2). The source attribution for these days was based on the chemical speciation data and using Eqs. 3 (FS), 4 (AS), 5 (MD), OM, EC, and non-SS sulfate to estimate the relative contributions to the total reconstructed mass (Eq. 6). Also included in the source attribution is the category "others" that represents the sum of other measured ion and elements not accounted for in the above categories. For each of the identified days, information will be presented on the source attribution and the characterization of the meteorology for the day (i.e., windroses, PM_{10} roses, and hours of the day that winds may be transporting PM_{10} towards the CDF monitoring site). The wind, PM_{10}-roses, and the attribution of the hours of PM_{10} transport from the direction of the ODSVRA to the CDF site are based on hourly measurements of wind speed and direction and hourly PM_{10} (as measured by a Beta Attenuation Monitor) for instruments operated by the APCD (data supplied to DRI by the APCD).

5/4/2021

On this date the gravimetrically determined PM_{10} concentration was 50 µg m^{-3}. The windrose shown in Figure 12 (top) indicates that on this day winds in excess of 2 m s^{-1} at the CDF site were predominantly from the west and west-north-west accounting for 58% of the 24 hours (wind direction from 236°-305°). The PM_{10}-rose (Figure 12 bottom) shows the direction of transport and the magnitude of the PM_{10} concentrations as a function of the directional range. For the directional range, 236°-305°, the mass contribution to CDF during this time represents 58% of the total mass measured. The source attribution

for this day is shown in Figure 13. Fresh and aged sea salts are the dominant PM_{10} constituents (48.5% and 8.8%, respectively), while mineral dust is 8.3% of PM_{10}.

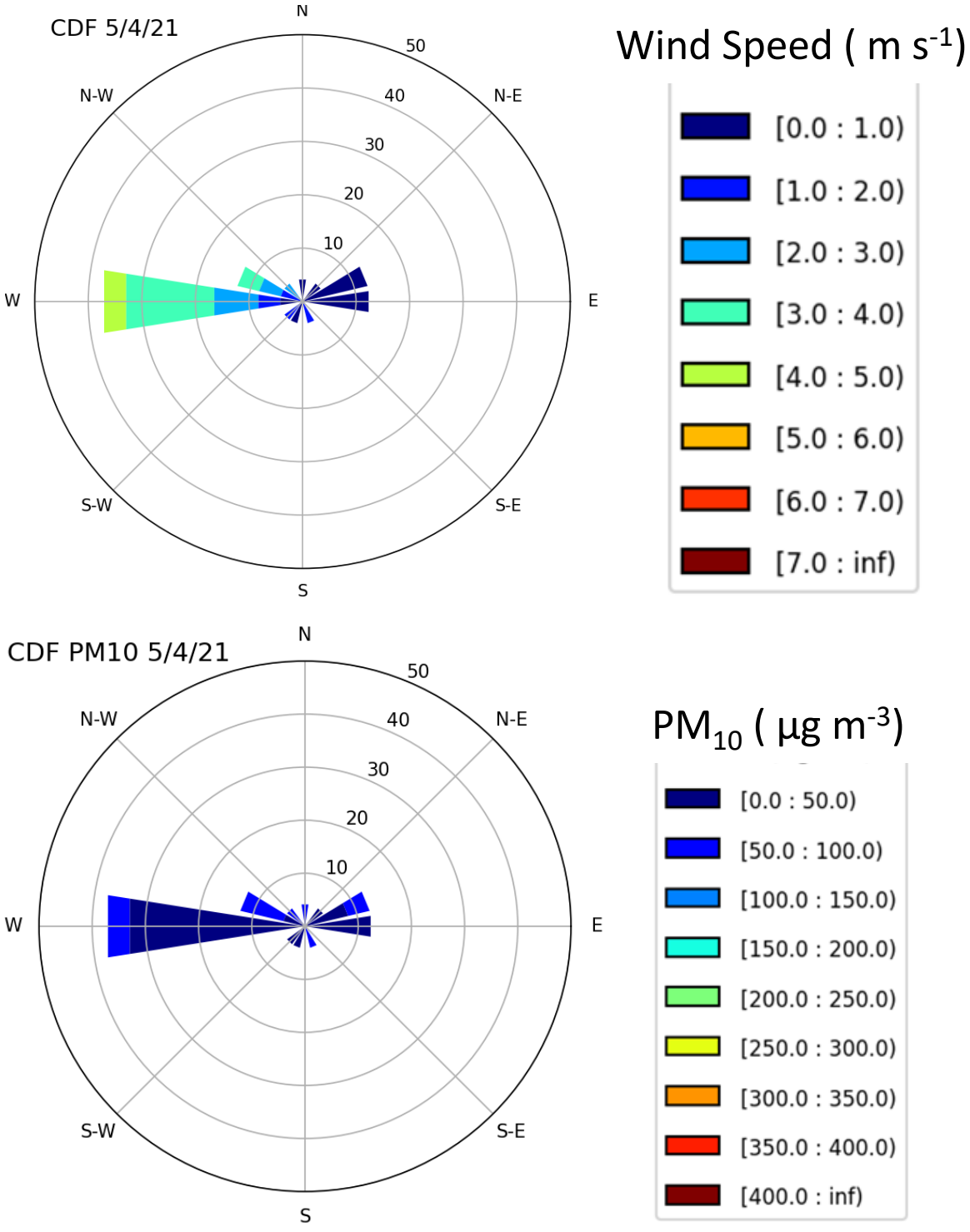

Figure *12*. The wind speed and PM_{10} concentration distributions by wind direction, 5/4/2021.

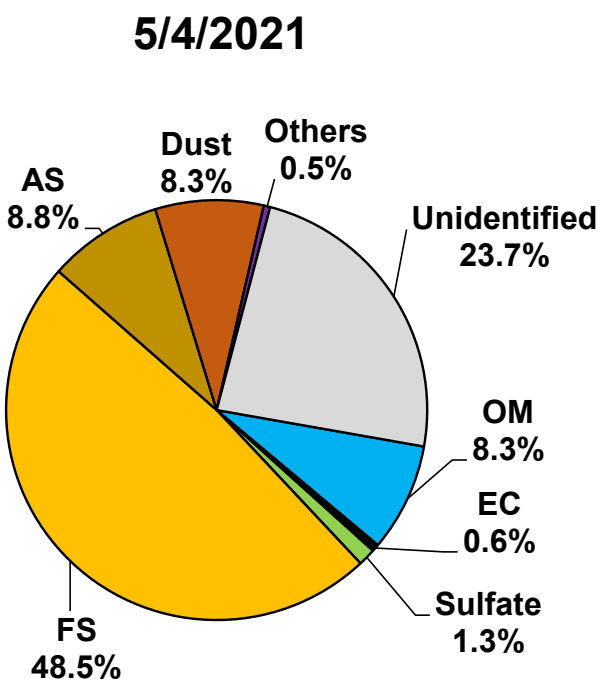

Figure *13.* The PM_{10} source attribution for 5/4/2021.

5/7/2021

On this date the gravimetrically determined PM_{10} concentration was 70 µg m^{-3}. The windrose shown in Figure 14 (top) indicates that on this day winds in excess of 2 m s^{-1} at the CDF site were predominantly from the west-north-west to north-west accounting for 71% of the 24 hours (wind direction from 268°-328°). The PM_{10}-rose (Figure 14 bottom) shows the direction of transport and the magnitude of the PM_{10} concentrations as a function of the directional range. For the directional range 268°-328°, the mass contribution to CDF during this time represents 84% of the total mass measured. The source attribution for this day is shown in Figure 15. Both sea salt (31.6%) and mineral dust (39.2%) are significant PM_{10} constituents.

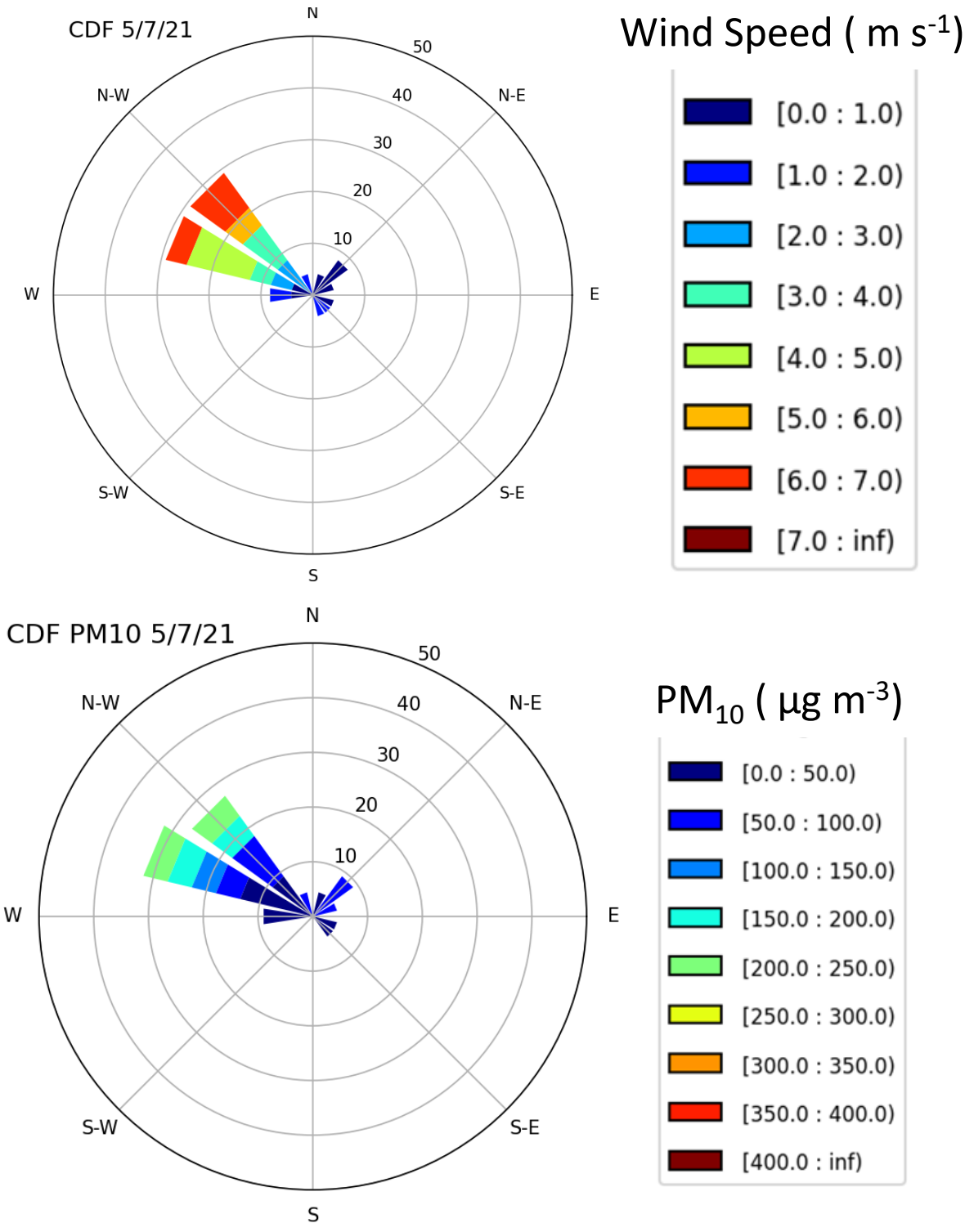

Figure 14. The wind speed and PM_{10} concentration distributions by wind direction, 5/7/2021.

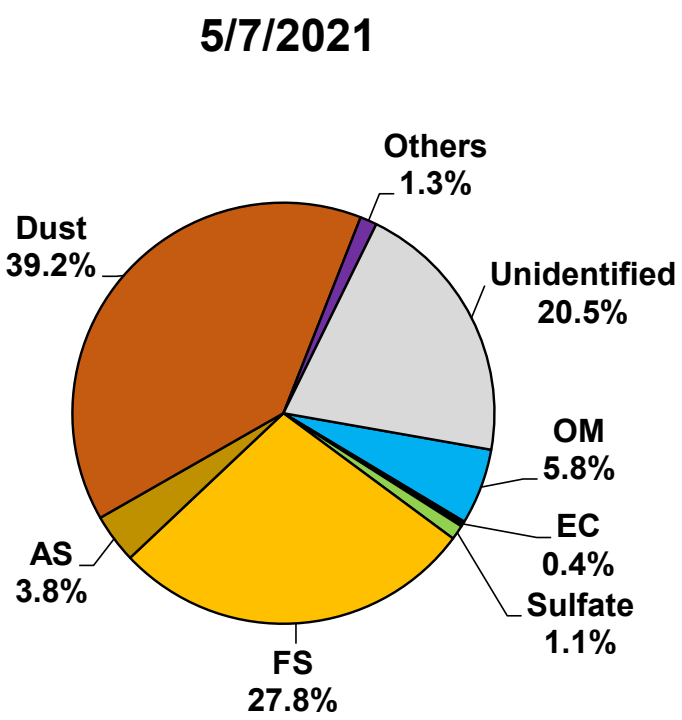

Figure 15. The PM_{10} source attribution for 5/7/2021.

5/19/2021

On this date the gravimetrically determined PM_{10} concentration was 103 µg m^{-3}. The windrose shown in Figure 16 (top) indicates that on this day winds in excess of 2 m s^{-1} at the CDF site were predominantly from the west-north-west to north-west accounting for 67% of the 24 hours (wind direction from 290°-332°). The PM_{10}-rose (Figure 16 bottom) shows the direction of transport and the magnitude of the PM_{10} concentrations as a function of the directional range. For the directional range, 290°-332°, the mass contribution to CDF during this time represents 89% of the total mass measured. The source attribution for this day is shown in Figure 17. Mineral dust is the dominant PM_{10} constituent (46.6%), while fresh and aged sea salts are 18.9% and 2.3% of PM_{10} mass, respectively.

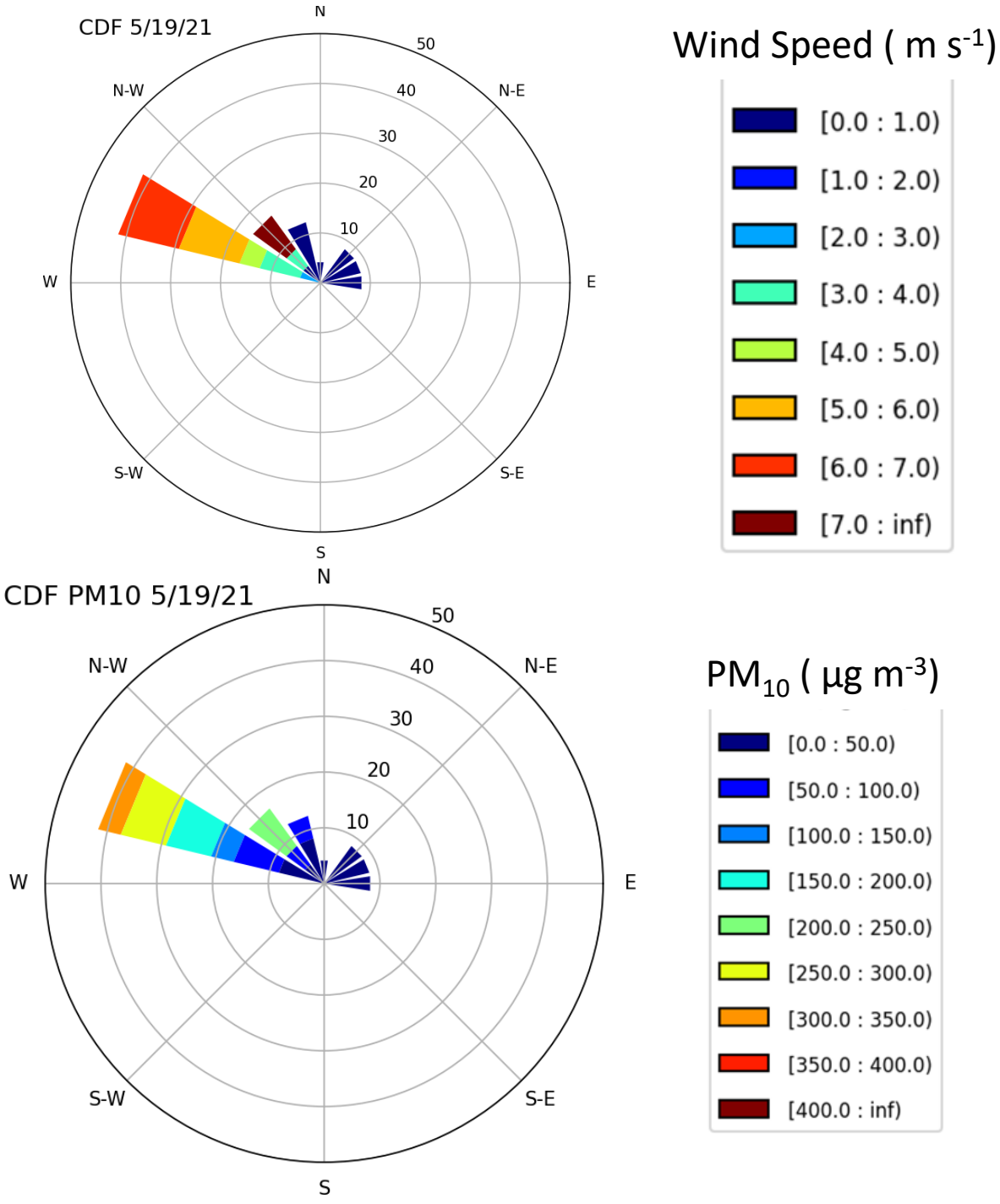

Figure 16. The wind speed and PM_{10} concentration distributions by wind direction, 5/19/2021.

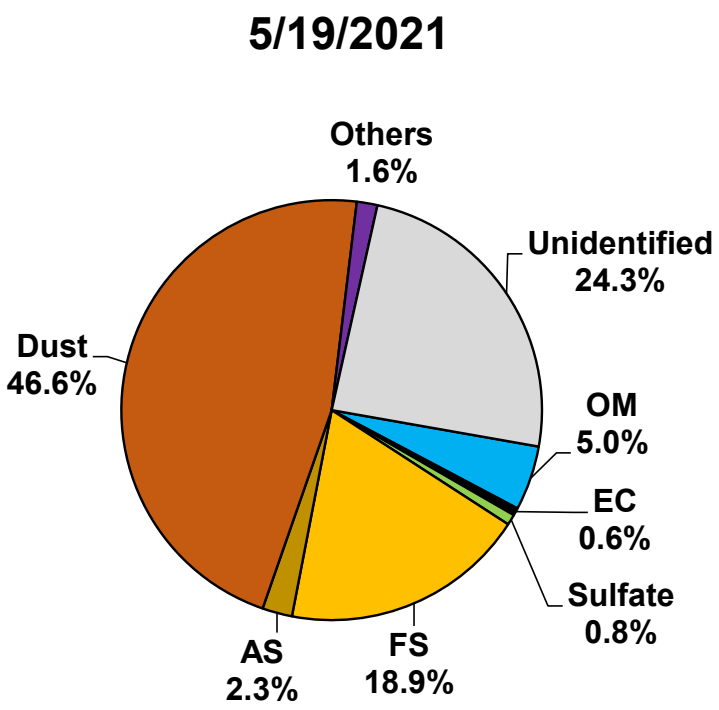

Figure 17. The PM_{10} source attribution for 5/19/2021.

6/12/2021

On this date the gravimetrically determined PM_{10} concentration was 61 µg m^{-3}. The windrose shown in Figure 18 (top) indicates that on this day winds in excess of 2 m s^{-1} at the CDF site were predominantly from the west-north-west to north-west accounting for 71% of the 24 hours (wind direction from 257°-336°). The PM_1-rose (Figure 18 bottom) shows the direction of transport and the magnitude of the PM_{10} concentrations as a function of the directional range. For the directional range, 257°-336°, the mass contribution to CDF during this time represents 93% of the total mass measured. The source attribution for this day is shown in Figure 19. Mineral dust is the dominant PM_{10} constituent (51.6%), while fresh and aged sea salts are 16.8% and 0.7% of PM_{10} mass, respectively.

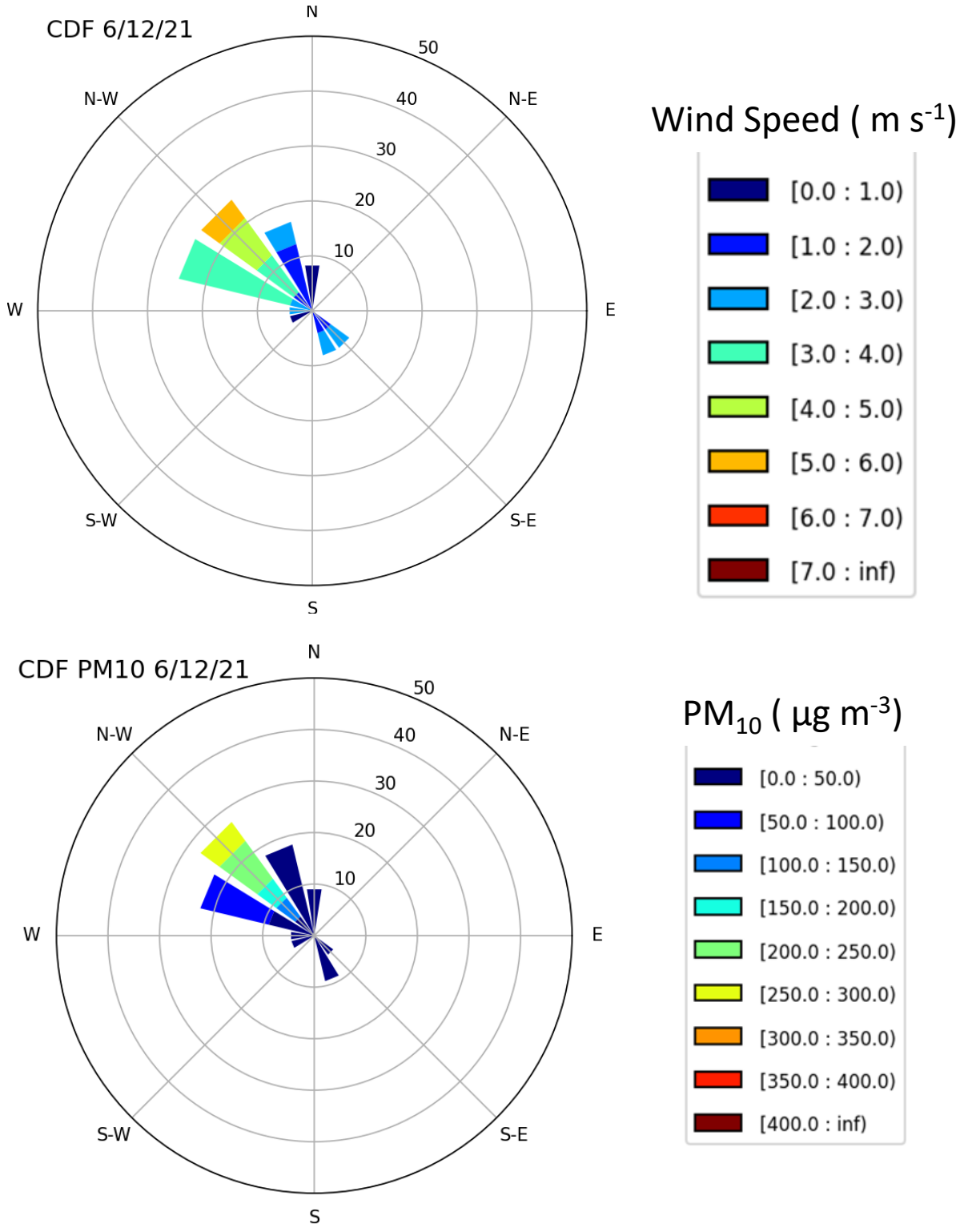

Figure 18. The wind speed and PM_{10} concentration distributions by wind direction, 6/12/2021.

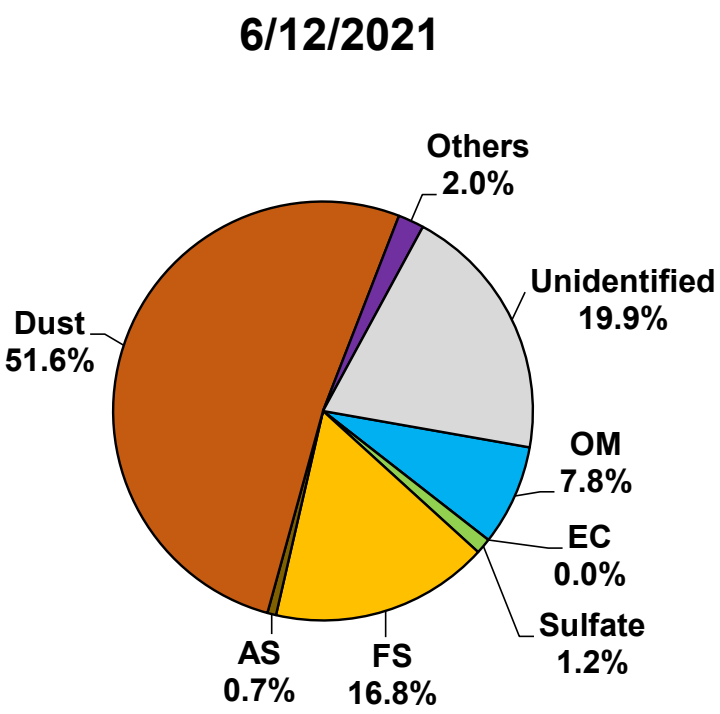

Figure 19. The PM_{10} source attribution for 6/12/2021.

6/15/2021

On this date the gravimetrically determined PM_{10} concentration was 90 µg m^{-3}. The windrose shown in Figure 20 (top) indicates that on this day winds in excess of 2 m s^{-1} at the CDF site were predominantly from the north-west to north-north-west accounting for 54% of the 24 hours (wind direction from 257°-336°). The PM_{10}-rose (Figure 20 bottom) shows the direction of transport and the magnitude of the PM_{10} concentrations as a function of the directional range. For the directional range, 257°-336°, the mass contribution to CDF during this time represents 93% of the total mass measured. The source attribution for this day is shown in Figure 21. Mineral dust is the dominant PM_{10} constituent (41.1%), but fresh and aged sea salts are also significant contributors (24.1% and 3.5% of PM_{10} mass, respectively).

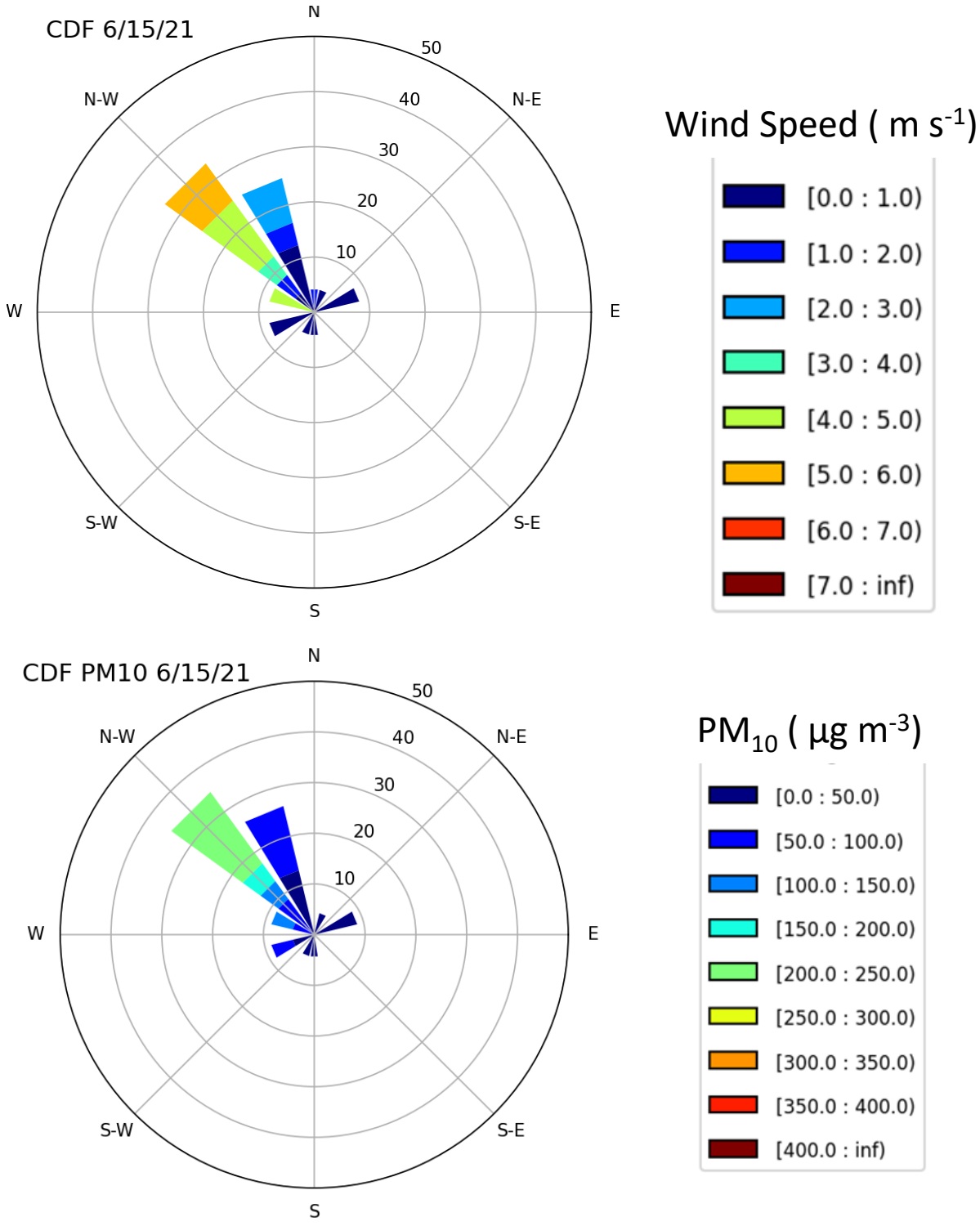

Figure 20. The wind speed and PM_{10} concentration distributions by wind direction, 6/15/2021.

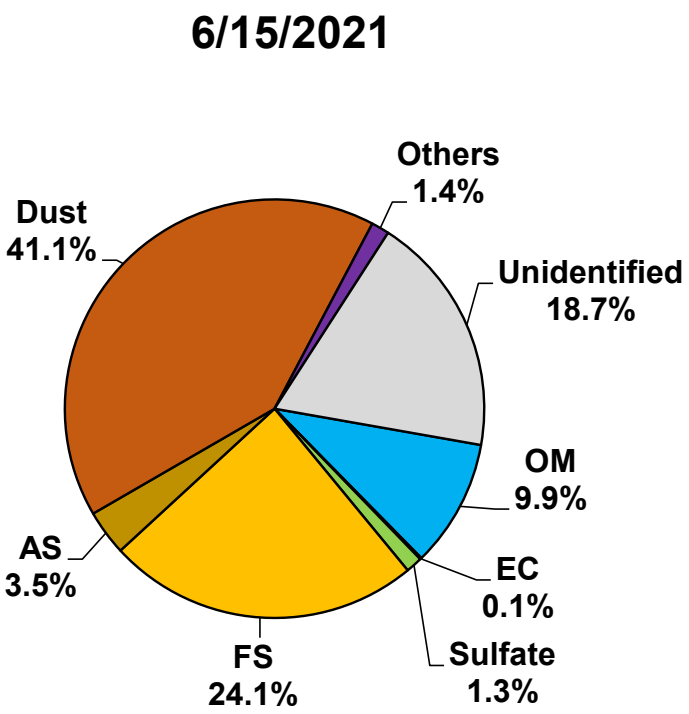

Figure 21. The PM_{10} source attribution for 6/15/2021.

9/19/2021

On this date the gravimetrically determined PM_{10} concentration was 78 µg m^{-3}. The windrose shown in Figure 22 (top) indicates that on this day winds in excess of 2 m s^{-1} at the CDF site were predominantly from the north-west accounting for 50% of the 24 hours (wind direction from 257°-336°). The PM_{10}-rose (Figure 22 bottom) shows the direction of transport and the magnitude of the PM_{10} concentrations as a function of the directional range. For the directional range, 257°-336°, the mass contribution to CDF during this time represents 85% of the total mass measured. The source attribution for this day is shown in Figure 23. Mineral dust is the dominant PM_{10} constituent (58.2%), while fresh and aged sea salts are 11.7% and 1.1% of PM_{10} mass, respectively.

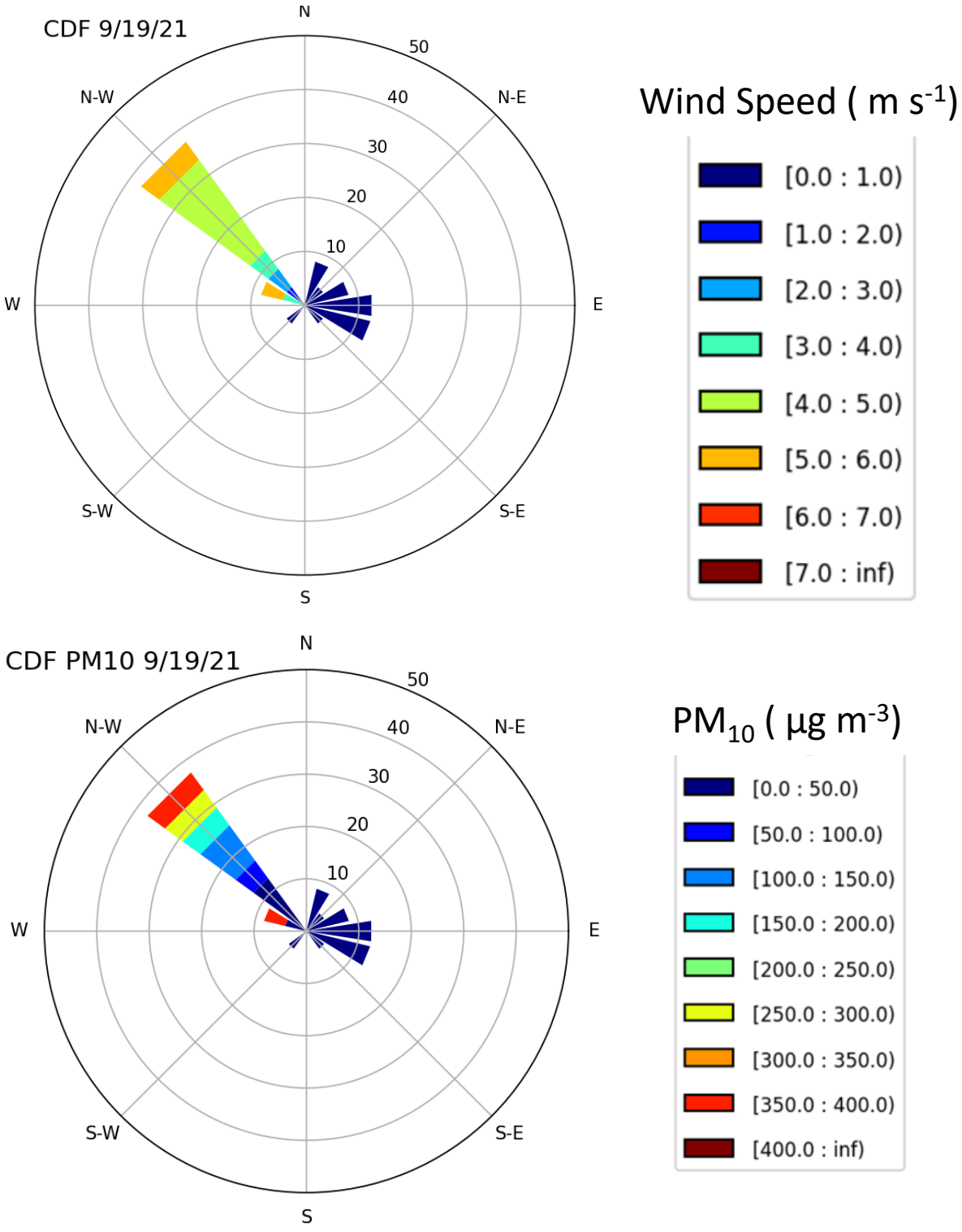

Figure 22. The wind speed and PM_{10} concentration distributions by wind direction, 9/19/2021.

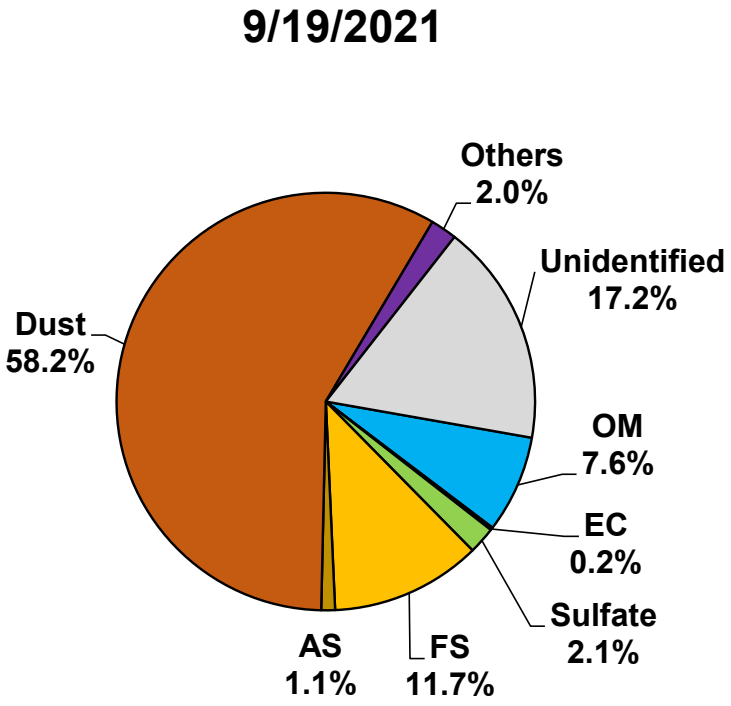

Figure 23. The PM_{10} source attribution for 9/19/2021.

9/28/2021

On this date the gravimetrically determined PM_{10} concentration was 82 µg m^{-3}. The windrose shown in Figure 24 (top), indicate that on this day winds in excess of 2 m s^{-1} at the CDF site were predominantly from the north-west to north-north-west accounting for 63% of the 24 hours (wind direction from 298°-330°). The PM_{10}-rose (Figure 24 bottom) shows the direction of transport and the magnitude of the PM_{10} concentrations as a function of the directional range. For the directional range, 298°-330°, the mass contribution to CDF during this time represents 92% of the total mass measured. The source attribution for this day is shown in Figure 25. Mineral dust is the dominant PM_{10} constituent (50%), while fresh and aged sea salts are 15.6% and 0.7% of PM_{10} mass, respectively.

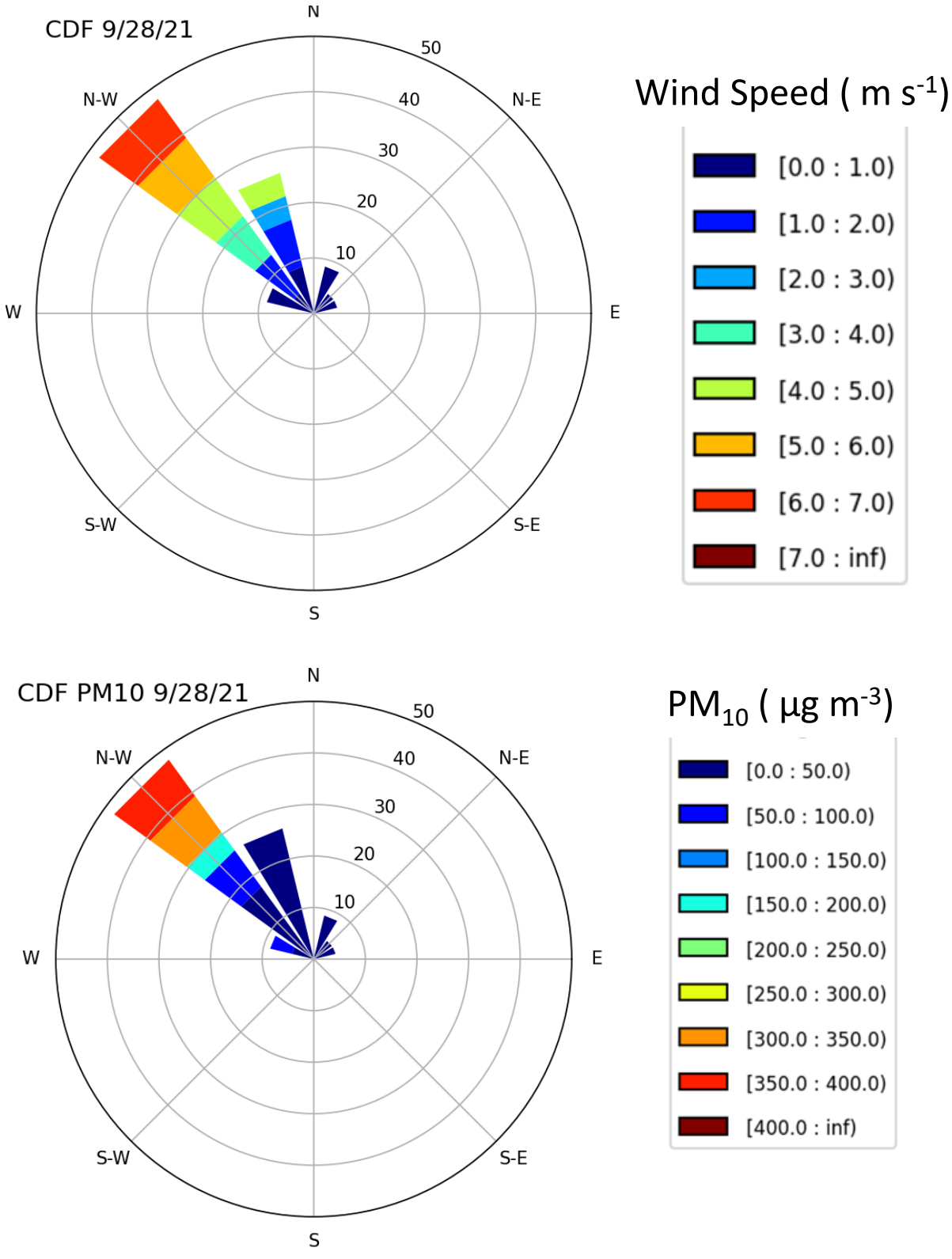

Figure 24. The wind speed and PM_{10} concentration distributions by wind direction, 9/28/2021.

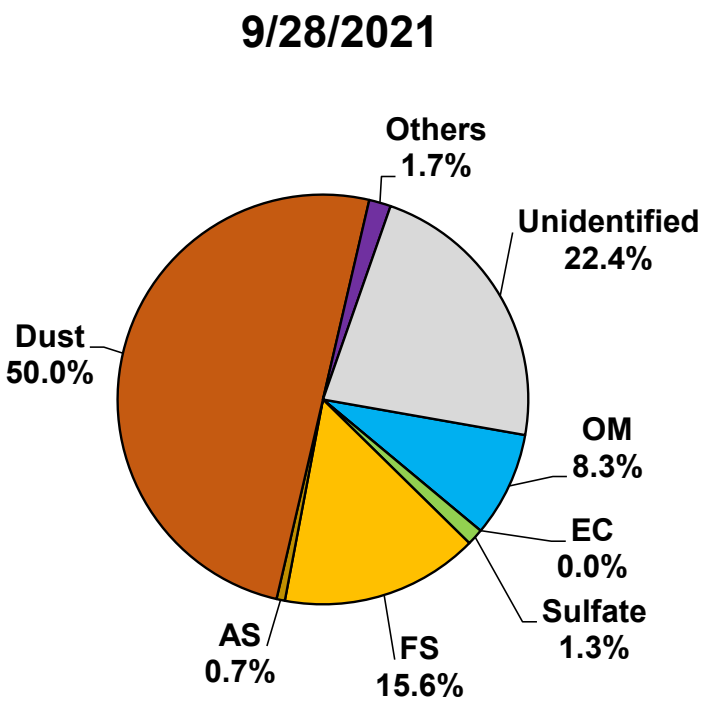

Figure 25. The PM_{10} source attribution for 9/28/2021.

10/13/2021

On this date the gravimetrically determined PM_{10} concentration was 53 µg m^{-3}. The windrose shown in Figure 26 (top), indicate that on this day winds in excess of 2 m s^{-1} at the CDF site were predominantly from the north-west accounting for 46% of the 24 hours (wind direction from 240°-315°). The PM_{10}-rose (Figure 26 bottom) shows the direction of transport and the magnitude of the PM_{10} concentrations as a function of the directional range. For the directional range, 240°-315°, the mass contribution to CDF during this time represents 61% of the total mass measured. This value is affected by the missing hourly PM_{10} value for 10:00 am to 11:00 am. Substituting the mean PM_{10} value from the previous and next hours (52 ±16 µg m^{-3}) for the 11:00 am missing value the mass contribution to CDF during this time would represent 63% of the total mass measured. The source attribution for this day is shown in Figure 27. The PM_{10} compositions are very similar to those of 9/28/2022: mineral dust is the dominant PM_{10} constituent (49.8%), while fresh and aged sea salts are 16.0% and 0.4% of PM_{10} mass, respectively.

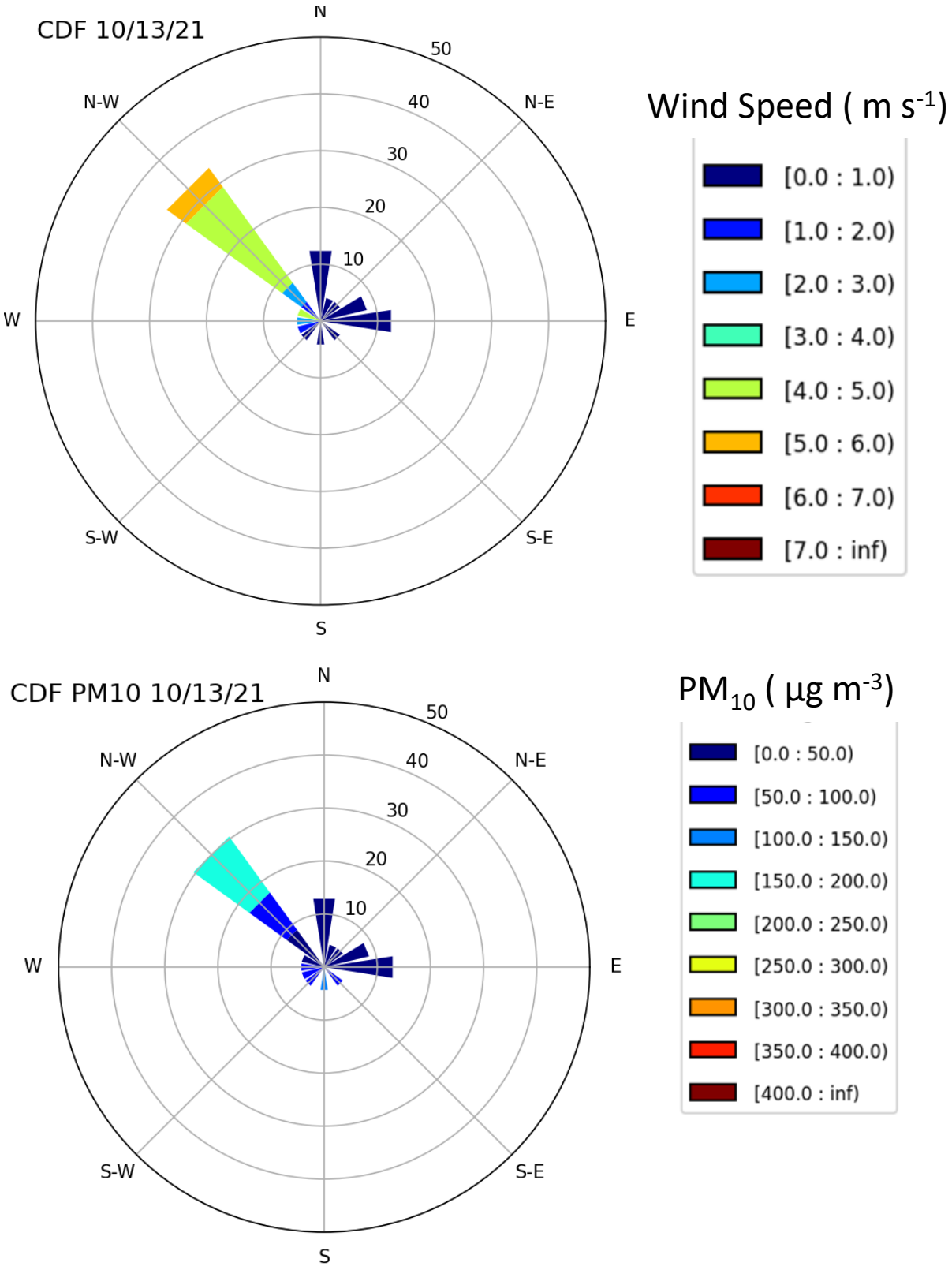

Figure 26. The wind speed and PM_{10} concentration distributions by wind direction, 10/13/2021.

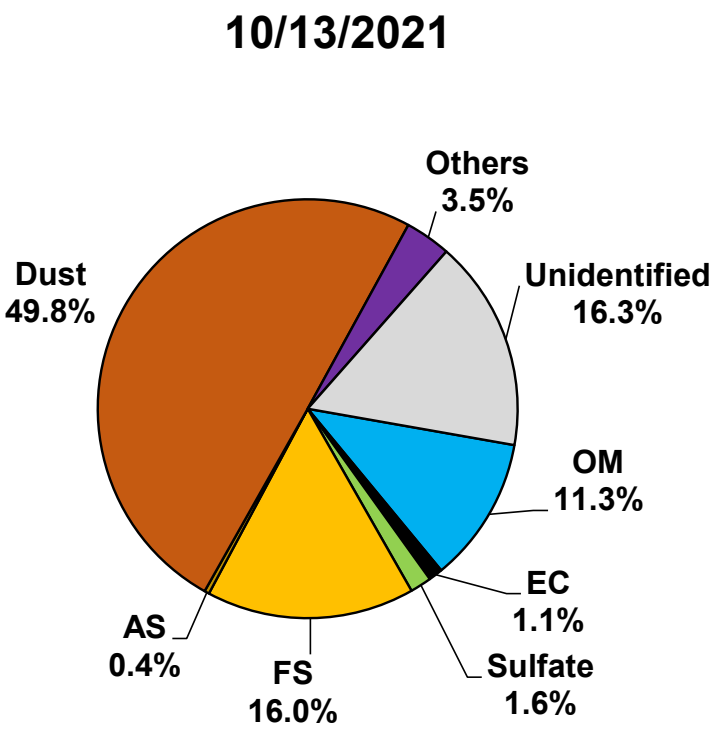

Figure 27. The PM_{10} source attribution for 10/13/2021.

Compiled Source Attribution for Exceedance Days in 2021

For the exceedance days identified for the period April-October 2021, for the sources defined for each individual day (excluding 10/7/2021), the percent composition from each of the pie charts were used to calculate a mean source attribution for an exceedance day. This attribution is presented in Figure 27. The dominant source of the PM_{10} as shown in Figure 28 is MD (43.1% ±15.3%) followed by SS (22.4% ±11.7% for FS and 2.6% ±2.8% for AS), and the unidentified category (20.4% ±2.9%).

The PM_{10} concentration contribution of MD and SS should increase as a function of wind energy and additionally for SS the size and frequency of the breaking waves. The other constituents are not affected by wind, and under higher wind speeds will be more efficiently dispersed, which will lower their concentration and contribution to total PM_{10} during a 24-hour period.

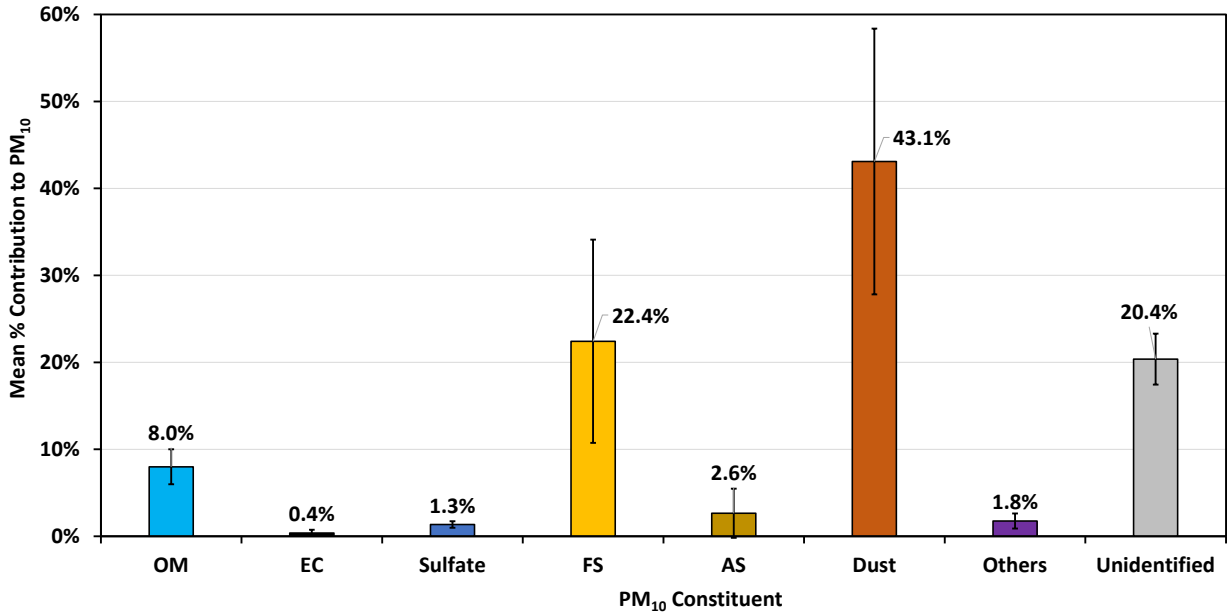

Figure 28. The mean source attribution of PM_{10} representing the eight exceedance days between May and October 2021.

The unidentified constituent of 20.4% (±2.9%) cannot be unambiguously resolved due to two analytical challenges. The first challenge is to account for the mass of PM_{10} that is related to the presence of the oxide components of minerals that are not resolved by XRF or the other analytical methods. The second challenge is to measure the particle-bound water content. The filters are weighed at 21.5 ±1.5 °C and 35 ±5% RH. This RH is lower than the efflorescence RHs of the main salt forms NaCl (43%), $NaNO_3$ (40%), and Na_2SO_4 (55%) (Martin, 2000); therefore, the salt particles are likely in a dry state. However, McInnes et al. (1996) observed that water made up 9% of submicron marine aerosol mass when weighted at 35% RH. Additionally, minerals often exist in hydrated phases, including water in the crystal structures (King et al., 2011). Currently there are no standard ways to accurately determine mineral compositions or particle-bound water content on aerosol samples. It is our opinion that most of the unidentified mass represents the oxide components of the quartz and feldspar minerals common to the sands of the Oceano Dunes along with the other less common elements (e.g., VA-U) that were identified by the XRF analysis, and less common minerals and their associated oxides. Equation 5 is a simplification for resolving a very generalized mineral dust that was developed for rural sites in the IMPROVE network and cannot be made specific to geographic area (Malm et al., 1994; Simon et al., 2011). We arrive at this conclusion as the wind and PM_{10} roses indicate that transport to the CDF site for the identified exceedance days is dominated by periods when the wind direction was from the ODSVRA and the ocean.

As the OM and EC components were quite low, there is no indication of combustion processes as a significant contributor. The low concentrations of methyl methanesulfonate ($CH_3SO_3^-$) indicate that biogenic components of PM_{10} originating from marine sources were insignificant on all sampling days. Other significant PM_{10} sources between CDF and the ODSVRA are implausible as upwind of CDF is mainly open vegetation covered areas until the eastern edge of the Oceano dunes are reached. Assuming the

"unidentified" constituent represents uncharacterized components of the mineral dust (i.e., the oxide components of the mineral particles), unidentified mass is most likely associated with mineral components of the PM_{10}, the mean attribution of MD for the data shown in Fig. 28 increases to 63.5% (±16%).

Compiled Source Attribution for Non-Exceedance Days in 2021

For the non-exceedance days identified for the period April-October 2021, for the sources defined for each individual day (excluding 10/7/2021), the percent composition from each day was used to calculate a mean source attribution for a non-exceedance day. This attribution is presented in Fig. 29.

The dominant source of the PM_{10} as shown in Fig. 29 is SS (FS, 29.7% ±15.6%, AS, 10.9% ±8.3%), followed by MD (24.3% ±14.6%), OM (22.4% ±16.9%), and the unidentified category (6.6% ±5.9%). The contributions from EC remain low, similar to the mean exceedance day contributions (Fig. 27). Sulfate increases as more sources are likely in inland areas than areas to the west of CDF. The source attribution for the mean non-exceedance day represents a day with low probability of winds that entrained sand and emitted dust within the ODSVRA as well as much greater degree of mixing with a wider range of wind direction. The non-exceedance day source attribution does not provide much useful information in terms of air quality management with respect to PM_{10} originating from the ODSVRA and reflects the regional attribution of sources when MD is not actively being emitted in the ODSVRA under conditions of elevated wind speeds for westerly winds.

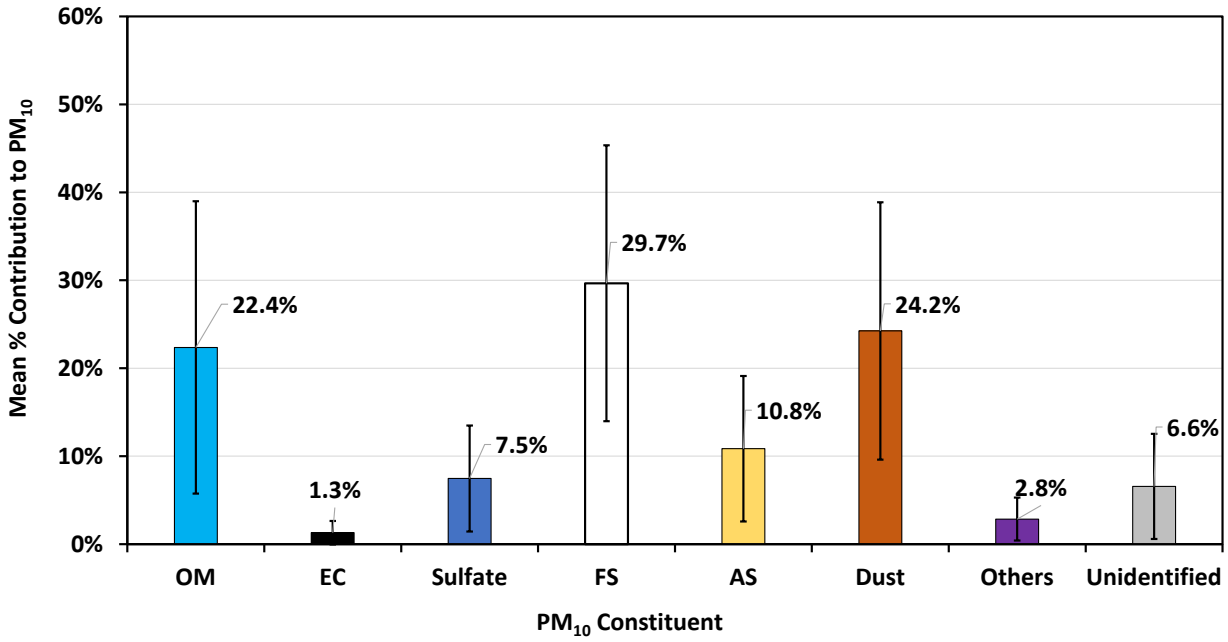

Figure *29*. The mean source attribution of PM_{10} representing the non-exceedance days between May and October 2021.

References

Bardouki, H., Liakakou, H., Economou, C., Sciare, J., Smoĺík, J., Ždímal, V., Eleftheriadis, K., Lazaridis, M., Dye, C., Mihalopoulos, N. (2003). Chemical composition of size-resolved atmospheric aerosols in the eastern Mediterranean during summer and winter. *Atmos. Environ.* 37 (2):195-208, doi: 10.1016/S1352-2310(02)00859-2.

Chen, L.-W.A., Chow, J.C., Wang, X.L., Robles, J.A., Sumlin, B., Lowenthal, D.H., Zimmermann, R., Watson, J.G. (2015). Multi-wavelength optical measurement to enhance thermal/optical analysis for carbonaceous aerosol. *Atmos. Meas. Tech.* 8:451-461, doi: 10.5194/amt-8-451-2015.

Cheung, K., Daher, N., Shafer, M.M., Ning, Z., Schauer, J.J., Sioutas, C. (2011). Diurnal trends in coarse particulate matter composition in the Los Angeles Basin. *J. Environ. Monit.* 13 (11):3277-3287, doi: 10.1039/C1EM10296F.

Chow, J.C., Watson, J.G., Chen, L.-W.A., Chang, M.C.O., Robinson, N.F., Trimble, D., Kohl, S. (2007). The IMPROVE_A temperature protocol for thermal/optical carbon analysis: maintaining consistency with a long-term database. *Journal of the Air & Waste Management Association* 57 (9):1014-1023.

Chow, J.C., Watson, J.G. (2013). Chemical analyses of particle filter deposits. In: Ruzer, L., Harley, N.H. (Eds.), *Aerosols Handbook : Measurement, Dosimetry, and Health Effects*, 2 ed. CRC Press/Taylor & Francis, New York, NY, pp. 179-204.

Chow, J.C., Lowenthal, D.H., Chen, L.-W.A., Wang, X.L., Watson, J.G. (2015). Mass reconstruction methods for $PM_{2.5}$: a review. *Air Quality, Atmosphere & Health* 8 (3):243-263. 10.1007/s11869-015-0338-3.

Chow, J.C., Watson, J.G. (2017). Enhanced ion chromatographic speciation of water-soluble $PM_{2.5}$ to improve aerosol source apportionment. *Aerosol Science and Engineering* 1:7-24. doi:10.1007/s41810-017-0002-4.

Environmental Analysis Facility (2017). Stand Operating Procedure 2-112r4, PM2.5 FRM Filter Pack Assembly, Disassembly, and Cleaning, Revision #4 (9/28/2017).

Environmental Analysis Facility (2018). Stand Operating Procedure 2-106r9, Pre-firing and Acceptance Testing of Quartz fiber Filters for Aerosol and Carbonaceous Material Sampling, Revision #9 (8/20/2018).

Environmental Analysis Facility (2020). Stand Operating Procedure 2-113r7, PM2.5 FRM Sample Shipping, Receiving, and Chain of Custody, Revision #7 (10/13/2020).

Environmental Analysis Facility (2021a). Stand Operating Procedure 2-114r14, PM2.5 FRM Gravimetric Analysis, Revision #14 (12/6/2021).

Environmental Analysis Facility (2021b). Stand Operating Procedure 2-109r13, X-ray Fluorescence (XRF) Analysis of Aerosol Filter Samples (Panalytical Epsilon 5), Revision #13 (2/2/2021).

Environmental Analysis Facility (2021c). Stand Operating Procedure 2-109r10, Extraction of Ionic Species from Filter Samples, Revision #10 (2/3/2021).

Environmental Analysis Facility (2021d). Stand Operating Procedure 2-235r0, Ions by IC on Dionex 5000+\6000, Revision #00 (2/3/2021).

Environmental Analysis Facility (2021e). Stand Operating Procedure 2-226r7, DRI Model 2015 Multi-Wavelength Thermal\Optical Carbon Analysis of Aerosol Filter Samples, Revision #7 (12/13/2021).

Hand, J.L., Copeland, S.A., McDade, C.E., Day, D.E., Moore, J., C.T., Dillner, A.M., Pitchford, M.L., Indresand, H., Schichtel, B.A., Malm, W.C., Watson, J.G., (2011). Spatial and seasonal patterns and temporal variability of haze and its constituents in the United States, IMPROVE Report V. Cooperative Institute for Research in the Atmosphere, Fort Collins, CO, http://vista.cira.colostate.edu/Improve/spatial-and-seasonal-patterns-and-temporal-variability-of-haze-and-its-constituents-in-the-united-states-report-v-june-2011/.

King, J., Etyemezian, V., Sweeney, M., Buck, B.J., Nikolich, G. (2011). Dust emission variability at the Salton Sea, California, USA. *Aeolian Res.* 3 (1):67-79.

Lowenthal, D., Kumar, N. (2006). Light scattering from sea-salt aerosols at Interagency Monitoring of Protected Visual Environments (IMPROVE) Sites. *J. Air Waste Manage. Assoc.* 56 (5):636-642. 10.1080/10473289.2006.10464478.

Malm, W., Sisler, J., Huffman, D., Eldred, R., Cahill, T. (1994). Spatial and seasonal trends in particle concentration and optical extinction in the United States. *J. Geophys. Res.* 99 (D1):1347-1370.

Martin, S.T. (2000). Phase transitions of aqueous atmospheric particles. *Chem. Rev.* 100 (9):3403-3454, doi: 10.1021/cr990034t.

McInnes, L.M., Covert, D.S., Quinn, P.K., Germani, M.S. (1994). Measurements of chloride depletion and sulfur enrichment in individual sea-salt particles collected from the remote marine boundary layer. *Journal of Geophysical Research: Atmospheres* 99 (D4):8257-8268, doi: 10.1029/93JD03453.

McInnes, L.M., Quinn, P.K., Covert, D.S., Anderson, T.L. (1996). Gravimetric analysis, ionic composition, and associated water mass of the marine aerosol. *Atmos. Environ.* 30 (6):869-884.

Pakkanen, T.A. (1996). Study of formation of coarse particle nitrate aerosol. *Atmos. Environ.* 30 (14):2475-2482, doi: 10.1016/1352-2310(95)00492-0.

Seinfeld, J.H., Pandis, S.N. (2012). *Atmospheric Chemistry and Physics: from Air Pollution to Climate Change*, 2nd ed. John Wiley & Sons.

Simon, H., Bhave, P.V., Swall, J.L., Frank, N.H., Malm, W.C. (2011). Determining the spatial and seasonal variability in OM/OC ratios across the US using multiple regression. *Atmos. Chem. Phys.* 11 (6):2933-2949, doi: 10.5194/acp-11-2933-2011.

Usher, C.R., Michel, A.E., Grassian, V.H. (2003). Reactions on mineral dust. *Chem. Rev.* 103 (12):4883-4940, doi: 10.1021/cr020657y.

Watson, J.G., Chow, J.C., Frazier, C.A. (1999). X-ray fluorescence analysis of ambient air samples. In: Landsberger, S., Creatchman, M. (Eds.), *Elemental Analysis of Airborne Particles*, Vol. 1. Gordon and Breach Science, Amsterdam, The Netherlands, pp. 67-96.

Watson, J.G., Chow, J.C., Engling, G., Chen, L.-W.A., Wang, X.L. (2016). Source apportionment: Principles and methods. In: Harrison, R.M. (Ed.), *Airborne Particulate Matter*: *Sources, Atmospheric Processes and Health*, Royal Society of Chemistry, London, UK, pp. 72-125.

Watson, J.G., Tropp, R.J., Kohl, S.D., Wang, X.L., Chow, J.C. (2017). Filter Processing and Gravimetric Analysis for Suspended Particulate Matter Samples. *Aerosol Science and Engineering* 1 (2):93-105, doi: 10.1007/s41810-017-0010-4.

Zhuang, H., Chan, C.K., Fang, M., Wexler, A.S. (1999). Formation of nitrate and non-sea-salt sulfate on coarse particles. *Atmos. Environ.* 33 (26):4223-4233, doi: 10.1016/S1352-2310(99)00186-7.